Received: 1 December 2021 | Accepted: 29 April 2022 | Published online: 27 May 2022

DOI: 10.1111/opo.13008

OPO THE COLLEGE OF OPTOMETRISTS

ORIGINAL ARTICLE

Catastrophe optics theory unveils the localised wave aberration features that generate ghost images

Sergio Barbero[1] | **Arthur Bradley**[2] | **Norberto López-Gil**[3] | **Jacob Rubinstein**[4] | **Larry Thibos**[2]

[1]Instituto de Óptica (CSIC), Madrid, Spain

[2]School of Optometry, Indiana University, Bloomington, Indiana, USA

[3]Instituto Universitario de Investigación en Envejecimiento, Universidad de Murcia, Murcia, Spain

[4]Department of Mathematics, Technion, Haifa, Israel

Correspondence
Sergio Barbero, Instituto de Óptica (CSIC), Madrid, Spain.
Email: sergio.barbero@csic.es

Funding information
Israel Science Foundation, Grant/Award Number: 890015; Ministerio de Ciencia e Innovación (Spain), Grant/Award Number: PID2020-113596GB-I00

Abstract

Monocular polyplopia (ghost or multiple images) is a serious visual impediment for some people who report seeing two (diplopia), three (triplopia) or even more images. Polyplopia is expected to appear if the point spread function (PSF) has multiple intensity cores (a dense concentration of a large portion of the radiant flux contained in the PSF) relatively separated from each other, each of which contributes to a distinct image. We present a theory that assigns these multiple PSF cores to specific features of aberrated wavefronts, thereby accounting optically for the perceptual phenomenon of monocular polyplopia. The theory provides two major conclusions. First, the most likely event giving rise to multiple PSF cores is the presence of hyperbolic, or less probably elliptical, umbilic caustics (using the terminology of catastrophe optics). Second, those umbilic caustics formed on the retinal surface are associated with certain points of the wave aberration function, called cusps of Gauss, where the gradient of a curvature function vanishes. However, not all cusps of Gauss generate those umbilic caustics. We also provide necessary conditions for those cusps of Gauss to be *fertile*. To show the potential of this theoretical framework for understanding the nature and origin of polyplopia, we provide specific examples of ocular wave aberration functions that induce diplopia and triplopia. The polyplopia effects in these examples are illustrated by depicting the multi-core PSFs and the convolved retinal images for clinical letter charts, both through computer simulations and through experimental recording using an adaptive optics set-up. The number and location of cores in the PSF is thus a potentially useful metric for the existence and severity of polyplopia in spatial vision. These examples also help explain why physiological pupil constriction might reduce the incidence of ghosting and multiple images of daily objects that affect vision with dilated pupils. This mechanistic explanation suggests a possible role for optical phase-masking as a clinical treatment for polyplopia and ghosting.

KEYWORDS
catastrophe optics theory, caustics, ghost images, polyplopia, wavefront aberration singular analysis

INTRODUCTION

Poor optical quality is classically described at the image plane by the amount of blur, which is typically quantified by the size of the point spread function (PSF) or attenuation and phase shifts in the optical transfer function (OTF).[1] Predictably, in the absence of retinal or neural pathologies, the magnitude of blur is a principal determinant of vision quality. However, in addition to blur associated with defocus and aberrations, human observers occasionally report seeing multiple images monocularly,[2] most often reporting two images (diplopia),[3,4] but sometimes three (triplopia)[5–7] or more (polyplopia).[8,9] Conventional metrics of image quality based on the PSF and OTF were not designed to measure the effects of polyplopia, which has prompted us to explore the possibility that analysis of caustics in the PSF will reveal ways to predict the presence and number of multiple images to be expected, for an eye with known wavefront aberrations.

Monocular multiple 'ghost' images of an extended object are expected if the PSF has multiple cores (or 'hot spots'), where the radiant flux is concentrated locally and the multiple cores are spatially separated from each other. This follows from the fact that the convolution of an object with a PSF comprised of several PSF cores is equal to the sum of convolutions with each core separately,[10] each of which produces an image in a slightly different location. For example, Figure 1 illustrates three images of a letter chart generated by a wavefront aberration, $W = C_2^0 Z_2^0 + 0.4 Z_2^{-2} + 0.1 Z_4^0$, for three defocus values: under-powered eye (top row, $C_2^0 = -0.3$ μm); a well-focused eye (middle row, $C_2^0 = 0$ μm); and an over-powered eye (bottom row, $C_2^0 = +0.3$ μm) and a 6-mm-diameter pupil. In this standard notation, C_n^m is the aberration coefficient for the Zernike circle polynomial Z_n^m of order *n*, frequency *m*.[11] For demonstration purposes, we assumed that the system is spatially invariant (i.e., isoplanatic) over the dimension of the object (eye chart with the 0.0 logMAR row marked with the red line).

Diplopia is most prominent in the top row of Figure 1, where the PSF has two cores separated diagonally by 5 arcmin, which matches the diagonal separation of ghost letters on the 0.0 logMAR acuity line. The legibility of letters is normally hampered by the overlapping of ghost images, but for this under-powered example, the images of the smaller letters are so widely spaced that they remain legible. When no defocus is added (Figure 1, middle row), the PSF has four small cores collinearly separated by <5 arc minutes, which produce four partially overlapping images, making the smaller letters more difficult to identify. The PSF for the over-powered eye has four larger PSF cores that do not generate visible polyplopia and result in superior legibility of letters compared with the well-focused example.

The examples of computed retinal images in Figure 1 provide insight into why patients have difficulty describing the nature and number of ghost images perceived for complicated objects such as letter charts. Indeed, detection of multiple images might be impossible for sinusoidal grating objects because the superposition of two gratings that differ only in position (i.e., spatial phase) is another sinusoidal grating. For these same

Key points

- Monocular polyplopia occurs when the eye's point spread function contains multiple spatially separate intensity cores ('hot spots').
- Specific caustic patterns, which can be predicted from localised regions of the eye's wave aberration function, are the most likely source of these multiple intensity cores.
- The number and location of these caustic patterns may be clinically useful biomarkers for the existence of polyplopia, and additionally to design possible mitigating clinical strategies.

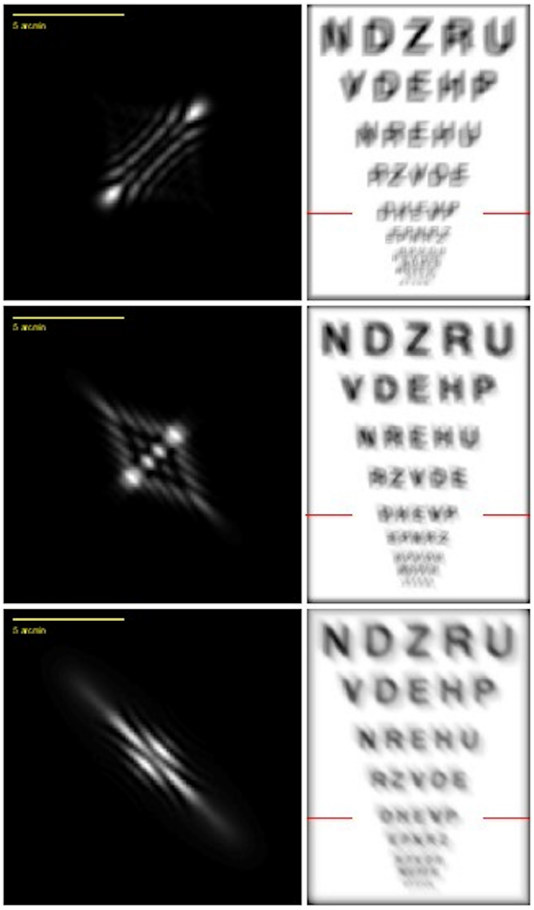

FIGURE 1 Example of multiple point spread function (PSF) cores inducing polyplopia. PSFs (left column) and computed retinal images (right column). Model wavefront aberration was $W = C_2^0 Z_2^0 + 0.4 Z_2^{-2} + 0.1 Z_4^0$, for three values of additional defocus: $C_2^0 = -0.3$ μm (top row), $C_2^0 = 0$ μm (middle row); and $C_2^0 = +0.3$ μm (bottom row). Pupil diameter = 6 mm. Red line identified the 0.0 logMAR letter size.

reasons, it is difficult to quantitatively assess ghosting by computational analysis of a retinal image even when the object is known. By comparison, it is much easier to identify and count the number of discrete, well-separated cores of concentrated light flux in the PSF, which is the method chosen for this study.

Early explanations of multi-core PSFs[2,12,13] identified caustics generated by aberrations as the likely underlying cause. The question we address in this paper is how to identify the specific features of the wave aberration of the human eye giving rise to these PSF cores. Specifically, we will use the wavefront error (WFE) function, which includes all of the eye's optical aberrations. We use this function to characterise caustics generated at the retina since these structures define regions of ray crossings and therefore higher flux density. Geometrical optics theory predicts infinite flux density at caustics,[14,15] just as it does at the focal plane of an aberration-free optical system, but the wave properties of light prevent such perfect and infinitesimally small focal points.[16] Wave optics reveals that the intensity along a caustic is not uniform,[17,18] being greater at some points than others.

The so-called catastrophe optics theory[17,19,20] provides a comprehensive theoretical framework to identify those singular points and their relative intensity, which is associated with the number of rays crossing each caustic point (within an asymptotic approximation to wave optics). In the following section, we briefly introduce catastrophe theory, which establishes that a limited number of events are responsible for the fragmentation of the PSF into multiple cores. A key idea that we introduce is that the eye's natural dynamics specifically defocus perturbations due, for instance, to accommodation fluctuations or even microfluctuations,[21] affect the character and number of such possible events. Depending on the amount of defocus, the intensity or even the number of PSF cores could be substantially modified, as we will demonstrate. Consequently, in a three-dimensional world with objects located at various distances, at any given moment in time, there might be polyplopia present for some objects but not for others because of their different viewing distances, hence different amounts of defocus.

In the section entitled 'Singular analysis of elementary catastrophe germs,' we identify the pupil-plane locations of the WFE function giving rise to PSF cores. Within the small slope approximation conventionally used in visual optics, caustics are generated by regions of the wavefront where the determinant of the vergence error matrix of the WFE function is zero (Equation 3).[15,18,20] Such regions of the wavefront are either isolated points or a set of connected points[22] and are called *critical* (or parabolic) points. Therefore, the desired wavefront regions associated with PSF cores must be included in, or at least be close to, the WFE critical points. In the singular analysis of elementary catastrophe germs, we algebraically derive the equations showing that those regions of interest are typically centred around certain points where the gradient of the determinant of vergence error matrix of the WFE function vanishes, called *cusps of Gauss*.[22,23] However, we note that not all cusps of Gauss generate PSF cores, as will be shown. We use the term *fertile* cusp of Gauss for those that do generate PSF cores.

To show the potential of these ideas for understanding the optical cause of polyplopia, we provide examples of WFE functions that induce diplopia and triplopia, respectively. Our method of identifying localised regions of the WFE responsible for producing PSF cores is applied to the problem of mitigating or eliminating polyplopia. Particularly, we show, through computational simulations, the capabilities of a phase-masking technique applied to the diplopia and triplopia examples introduced. We report experimental evidence of the previous theoretical predictions of polyplopia generation using an adaptive optics set-up with a deformable mirror and a recording charged-coupled device (CCD) sensor. Finally, we review and discuss our main results.

CATASTROPHE THEORY FOR UNDERSTANDING THE ORIGIN OF POINT SPREAD FUNCTION (PSF) CORES

Catastrophe theory was developed in the mid-1960s by René Thom[24] and later expanded by Vladimir I. Arnold and others.[25] Thom's interest was to develop a theory to describe and predict the genesis of typical shapes of living organisms. This is an example of the type of systems studied by catastrophe theory: those that can suffer sudden changes by smooth variations in certain parameters. In such systems, it is of obvious interest to understand when the system configuration is so-called *structurally stable*, namely, an equilibrium status where the qualitative behaviour of the system is unaffected by small perturbations. One of the most powerful results obtained from catastrophe theory (Thom's theorem) is that the number of possible structurally stable configurations is finite, and additionally, this number is only a function of the number of control parameters.[19] Furthermore, these structurally stable configurations can be classified hierarchically. Soon, it was realised that the theory could be applied to many different fields, including natural and social sciences. One of the first fertile fields of application was optics, particularly in describing and classifying caustics; this was extensively developed by Michael Berry and John F. Nye.[17,20] We note in passing that catastrophe optics is experiencing a revival in some branches of optics, particularly in what is called structured light or nondiffractive beams.[26,27]

Catastrophe theory enables classifying the type of structurally stable caustics. In most optical applications, the number of control parameters equals the number of coordinates describing an observation point at the image space: three (including through-focus analysis) or two (if

an observation plane is fixed, such as that of the retinal location). One of the surprising results of catastrophe theory is that, with three control parameters, there are only five structurally stable types of caustics called: *fold*, *cusp*, *swallowtail*, *elliptic* and *hyperbolic umbilics*.[19] We note that there are caustics involving certain symmetries, such as a rotational symmetry induced by combinations of defocus and spherical aberration, they are not structurally stable, and then, they do not fall under Thom's theorem. The five structurally stable caustics are hierarchically classified in terms of the intensity associated with them. There are two associated indices describing peak intensities and rate of intensity decay in the local vicinity.[17,20] Arnold's index provides information on the peak intensity value, and Berry's index measures the spacing of the first fringe (area of the first peak intensity). Arnold's index is related to the number of rays crossing at the caustic (the greater the number of rays crossing, the greater the intensity peak): two and three, for the fold and cusp caustics, and four for the swallowtail, elliptic and hyperbolic umbilics, respectively.[28] More specifically, the peak intensity is proportional to $\left(\frac{1}{\lambda}\right)^{\beta}$, where λ is the wavelength, and β is 1/6, 1/4, 3/10, 1/3 and 1/3 for the fold, cusp, swallowtail, elliptic and hyperbolic umbilics, respectively.[17,29] Thus, the peak intensities associated with elliptic and hyperbolic umbilics are the square of the fold, a relevant fact, as will be seen later on, when we identify those catastrophes relevant to generating PSF cores.

In human eye dynamics, the image plane (i.e., the planar approximation to the retinal surface) is not always located in the plane of best focus, changing its relative location through, for instance, lens accommodation. Within catastrophe theory, defocus due to differences between target vergence and the eye's refractive state causes the caustic surfaces to be intersected by the image plane at different locations along the optical axis, thereby changing the spatial features of the retinal point spread function. For example, the interaction of spherical aberration with defocus produces circular caustics centred on the optical axis because both aberrations are rotationally symmetric. The presence of asymmetric aberrations is required to produce starbursts and multiple cores, the latter being the topic of this report.

In this section, we use the terminology of catastrophe theory to describe the caustic curves generated by these intersections for each of the five aforementioned elementary catastrophes. In the next section, we shall derive the algebraic equations for the different elementary caustics.

Fold caustics are smooth surfaces (no discontinuities in the first derivative) like the one shown in Figure 2a in red. Intersecting such a surface with an arbitrary plane ($z = F$) provides a straight caustic line. Slightly moving around the image plane ($z = F \pm \delta$) still induces a single straight caustic line. Cusp caustics are smooth surfaces except at a straight line embedded on the surface where the surface does not have a continuous first derivative. At that line, the surface folds as shown in Figure 2b. The intersection of the image plane with the cusp surface at the singular location $z = F$ provides, as the fold caustic, a straight caustic line. The sign of defocus determines the direction of displacement of the image plane, which yields either two ($z = F + \delta$ at Figure 2b) or zero ($z = F - \delta$ at Figure 2b) straight caustic lines.

Swallowtail, elliptic and hyperbolic umbilic catastrophes are double-sheet caustic surfaces that coalesce at a unique point corresponding to an umbilical point, where the principal curvatures (i.e., the maximum and minimum of the normal curvature at a given point) of the wave aberration are equal. When the image plane contains that umbilical point, we say it is located at its 'best focal plane' because it is the plane of maximum flux concentration (i.e., irradiance). In this report, we refer to any other image plane as an 'out-of-focus' plane.

The shape of the swallowtail surface is complicated because it involves the crossing of two fold-type surfaces (whose intersection does not involve new catastrophes because the coalescing rays come from distinct parts of the wavefront).[20] Due to its shape complexity, we do not display it here and refer the reader to Nye.[20] As we will prove, the intersection of the swallowtail caustic with an image plane always produces single straight caustic lines regardless of the degree or sign of defocus.[18,30,31]

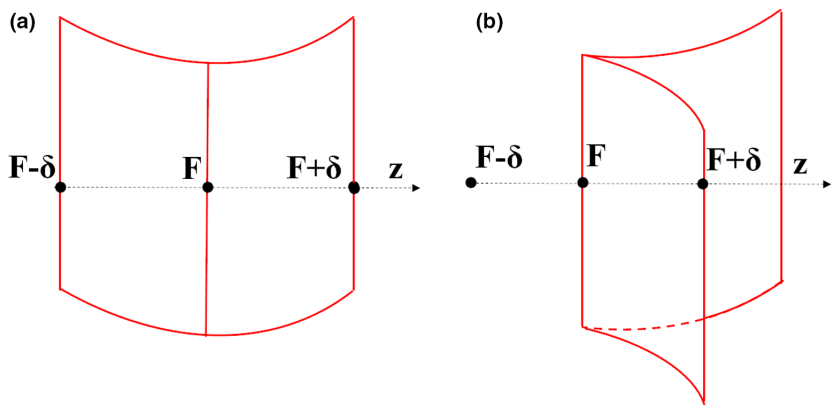

FIGURE 2 (a) Fold caustic. Caustic straight lines at planes $F - \delta$, F and $F + \delta$; (b) cusp caustic. No caustic line at plane $F - \delta$. One caustic straight line at F. Two caustic straight lines at $F + \delta$.

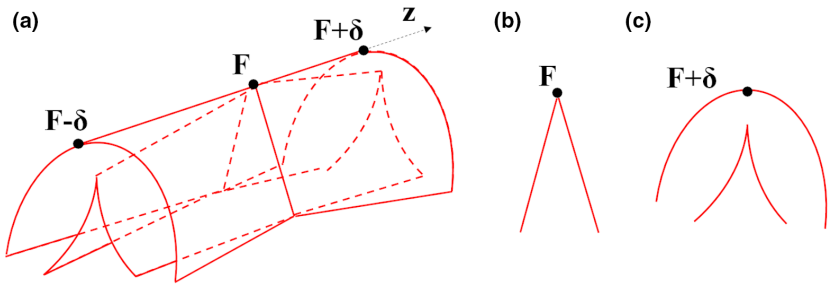

FIGURE 3 (a) Hyperbolic umbilic caustic shape; (b) caustic intersection at F; (c) caustic intersection at F + δ plane.

The hyperbolic umbilic caustic double-sheet surface is shown in Figure 3. The two sheets are equal at the best focal plane (z = F), and then, the caustic lines at that plane are two crossing straight lines (Figure 3b). The caustic surface is mirror-symmetric with respect to the best focal plane. Therefore, cutting the caustic surface with out-of-focus planes (z = F ± δ) provides two types of caustic curves (Figure 3c), a smooth caustic line and a curve containing a cusp. The distance between these caustic lines depends on the separation δ between the best focal and the out-of-focus plane.

Finally, the elliptical umbilic caustic double-sheet surface is shown in Figure 4. At the best focal plane, there is an isolated caustic point. As in the case of the hyperbolic umbilic caustic, there is mirror symmetry with respect to the best focal plane, but now, cutting the caustic surface with out-of-focus planes (z = F ± δ) provides deltoid-type caustic curves.

We note that these elementary caustics are *local events*, meaning that they are induced by localised regions of the wave aberration function, not necessarily at the pupil centre, as demonstrated in the singular analysis of elementary catastrophe germs. No matter how complicated the wavefront aberration function, as long as it can be described by a smooth function (continuously differentiable, such as a Zernike polynomial expansion), there are always a limited number of possible caustic catastrophes in a local neighbourhood. Moreover, in the presence of realistic human eye wave aberrations, it is very unlikely that the retinal plane cuts the localised caustics precisely and stably at its best focal planes. Therefore, the highest intensity peaks associated with the coalescence points of the hyperbolic and elliptical umbilic caustics are unlikely to occur in human eye PSFs.

Fold caustics provide the smallest of all the caustic catastrophe intensities and hence are the least likely to produce a clearly perceived PSF core. Cusp caustics degenerate into two separated parallel caustic lines under small out-of-focus perturbations, thus splitting an already not too bright intensity caustic. Conversely, the swallowtail catastrophes have high-intensity spread along a line, and thus are not good candidates to produce an isolated PSF core. Therefore, at the retina, the PSF cores are most likely associated with either the elliptical or the hyperbolic umbilical caustics. The latter is expected to generate a PSF core, provided the distance between both curves (related to the amount of defocus) is not long enough to separate the peak intensity fringes (Berry index) associated with the cusp and the fold. Then, the intensity of two crossing rays (folds) is combined with that of the three crossing rays (cusps). On the contrary, the three cusps of the deltoid generated by the out-of-focus elliptical umbilical caustic have significantly less intensity peaks (three crossing rays), unless they are so close as to be indistinguishable, then adding the effect of nine crossing rays. Therefore, we hypothesise that the PSF cores in natural eye wave aberrations will be generated by localised out-of-focus hyperbolic umbilical caustics and, less probably, very small out-of-focus elliptical umbilical caustics. In the singular analysis of elementary catastrophe germs, we derive the local algebraic and geometric features associated with these caustic singularities.

SINGULAR ANALYSIS OF ELEMENTARY CATASTROPHE GERMS

In conventional wave aberration analysis, the polynomial expansion is carried out around a coordinate reference centred around a chief ray, which in many cases, but not always, is the ray passing through the pupil centre and intersecting the retina. Such a procedure implicitly assumes that there is only one major PSF core localised around that coordinate centre. However, in the presence of multiple PSF cores, such an approximation is no longer convenient. Here, we analyse the local geometrical properties of the wave aberration that produces a structurally stable caustic as defined above, in the introduction to catastrophe theory for understanding the origin of PSF cores. These elementary wave aberrations are called germs in catastrophe theory.

Let us denote (x, y) the coordinates of a wavefront germ and its associated ray at the eye's exit pupil and (x', y', z') the coordinates of the ray's intersection with the observation (retinal) plane. Also, f′ denotes the paraxial image focal length of the wavefront germ. Then, the optical path length between the ray at the retina and the exit pupil, in the far-field approximation, is given by[20,32]:

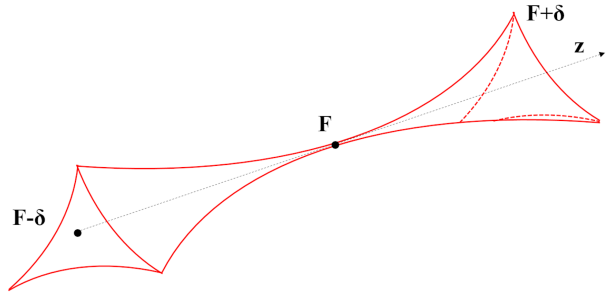

FIGURE 4 Elliptical umbilic caustic shape. Whereas intersection at F plane provides an isolated cusp point, at F ± δ provides a deltoid curve.

$$\emptyset(x,y,x',y') = W(x,y) + \frac{1}{2}\left(\frac{1}{z'} - \frac{1}{f'}\right)(x^2+y^2) + \frac{xx'}{z'} + \frac{yy'}{z'}, \tag{1}$$

where $W(x,y)$ is the corresponding germ of the WFE.

Following,[20,32] we use as control parameters the coordinates: $\xi = \frac{x'}{z'}, \eta = \frac{y'}{z'}$, and $\delta = \frac{1}{2}\left(\frac{1}{z'} - \frac{1}{f'}\right)$. In far-field approximation (valid for the human eye), x' and y' are small compared with z' so the control parameters ξ and η are approximately equal to the visual angles subtended at the exit pupil centre by the ray's intersection point with the retina.[15] Control parameter δ is half of the defocus, that is vergence difference of the wavefront germ with respect to the perfect wavefront focusing at the paraxial focus located f' from the exit pupil. We note that we choose half of the defocus, instead of just defocus, in order to be consistent with previous mathematical developments.[20,32]

Fermat's principle establishes that ray equations are given by those places where the optical path length $\emptyset(x,y,x',y')$ is stationary with respect to (x,y). The stationary points are those where $\frac{\partial \emptyset(x,y,x',y')}{\partial x} = \frac{\partial \emptyset(x,y,x',y')}{\partial y} = 0$. Then, applying these conditions on Equation (1) with the new control variables, we obtain (see also[18,20,32])

$$\xi = \frac{-\partial W}{\partial x} - x(2\delta), \eta = \frac{-\partial W}{\partial y} - y(2\delta). \tag{2}$$

Equation (2) provides a mapping between (x,y) points of the wave aberration at the exit pupil and angular coordinates (ξ,η) of the corresponding ray intersections with the retina.

Ray-mapping Equation (2) was obtained by imposing first-order stationary condition (zero gradient) to $\emptyset(x,y,x',y')$. To find caustics, $\emptyset(x,y,x',y')$ must be stationary to higher order than first order, which is found by differentiating Equation (2) with respect to x and y. Following Nye,[20] we obtain

$$det\begin{bmatrix} \frac{\partial^2 W}{\partial x^2} + 2\delta & \frac{\partial^2 W}{\partial xy} \\ \frac{\partial^2 W}{\partial xy} & \frac{\partial^2 W}{\partial y^2} + 2\delta \end{bmatrix} = 0. \tag{3}$$

Equation (3) is the classical condition determining the critical set at the exit pupil.

Denoting the left-hand side of Equation (3) as $G(x,y)$, we recognise G as the Gaussian curvature function of W when $\delta = 0$. Since W is a smooth function in the visual optics context, the implicit function theorem[33] implies that through every point (x,y) where $G(x,y) = 0$ and $\nabla G(x,y) \neq 0$, there passes a unique curve on which $G = 0$. This set of curves forms the critical set at the exit pupil. The mapping provided by Equation (2) transforms these curves into the caustic curves at the retinal plane.

We emphasise that the function $W(x, y)$ in Equation (3) is a wavefront error function (WFE) equal to the difference between an optical wavefront and a reference sphere centred on the image screen. The analysis of wave aberration functions frequently employs the so-called Gaussian reference sphere, for which the centre of curvature lies in the Gaussian image plane.[34] For example, a perfectly spherical wavefront of light has non-zero curvature at all points in the exit pupil, but the corresponding WFE associated with the Gaussian reference sphere is $W(x, y) = 0$, which is a plane with zero curvature everywhere. In this case, the entire optical wavefront contributes to a point caustic, that is the focal point. However, in this report we also employ non-Gaussian reference spheres because we wish to include the effects of defocus that arise when the retina is not conjugate with the object point. Thus, for the above example of a perfectly spherical wavefront in a defocused eye, $W(x, y) = \mathrm{A}\, r^2$, where A is a non-zero constant. In this case, no points exist for which $G(x, y) = 0$, so the defocused retinal image will be a uniform blur disk, which contain no caustics. These examples are consistent with previous reports that the magnitude and sign of defocus plays an important role in determining whether caustics and polyplopia are present in a retinal image.[35]

One way to locate candidates for PSF cores is to compute the critical curves at the exit pupil, and then their mapping according to Equation (2). However, this requires inverting the algebraic Equation (2). We therefore propose an alternative shorter way to find the PSF cores by using only the WFE at the exit pupil. An important advantage of locating the points at the exit plane giving rise to PSF cores will be clarified below, where we propose a means to alleviate the negative effect of polyplopia by blocking light coming from certain parts of the exit pupil.

It is known that cusp caustics are associated with ridge points of the wavefront, that is points along lines of curvature where one of the principal curvatures reaches a maximum or minimum.[17,22] The computation of these points is not a simple task (see, for instance, discussion in Barbero and Gonzalez36). Instead, we argue below that PSF cores can be associated with certain isolated cusps of Gauss,[22,23] defined as isolated points where $\nabla G(x,y) = 0$, that is where a necessary condition is the gradient of the determinant of the vergence error matrix for the WFE function vanishes:

$$\nabla\left(det\begin{bmatrix}\frac{\partial^2 W}{\partial x^2}+2\delta & \frac{\partial^2 W}{\partial xy}\\ \frac{\partial^2 W}{\partial xy} & \frac{\partial^2 W}{\partial y^2}+2\delta\end{bmatrix}\right)=0, \quad (4)$$

However, this is not the only necessary condition, as will be shown later on.

To understand why cusps of Gauss provide a useful tool to identify PSF cores, we now list the algebraic equations for the critical set, caustic lines and cusps of Gauss for each of the five elementary catastrophes. Table 1 provides the equations for the germs of the five elementary catastrophes (adapted from Nye[20]), their critical sets and the cusps of Gauss associated with them.

Table 2 provides the equations for the wave aberration germs of the five elementary catastrophes, their critical set and the cusps of Gauss associated with them.

Figure 5 shows the curvature *G* function maps for each elementary catastrophe and an out-of-focus perturbation of it (we choose $\delta = 0.5\,\mathrm{mm}^{-1}$). The critical set is plotted with red lines and the cusp of Gauss with green dots or lines.

The critical set in the fold catastrophe is a straight line, and no cusp of Gauss is present. Changing the observation plane location simply displaces the critical line. In the cusp catastrophe, both the critical set and the cusp of Gauss are a straight line ($x = 0$) passing through the centre of reference of the germ. When an out-of-focus perturbation is induced, the critical line is either duplicated and shifted or completely disappears (depending on the sign of δ). The critical set and cusp of Gauss in the swallowtail catastrophe are the same as that in a cusp case: a critical straight line passing through ($x = 0$) the centre of reference of the germ. However, in this case, an out-of-focus perturbation always induces a shifted critical straight line independently of the sign of the focus displacement. In the hyperbolic umbilical catastrophe, the critical set comprises crossing straight lines at a cusp of Gauss, which is also an umbilical point. When an out-of-focus perturbation is introduced, the critical lines change into a pair of hyperbolic curves, and the cusp of Gauss is laterally shifted a distance proportional to the defocus term. Finally, the elliptical umbilical catastrophe only contains an isolated critical point that is additionally an umbilical point and a cusp of Gauss. When an out-of-focus perturbation is introduced, an elliptical critical curve appears, and the cusp of Gauss is laterally shifted a distance proportional to the defocus term.

TABLE 1 Wavefront error function (WFE) germs, its critical sets and the cusps of Gauss for the five elementary catastrophe caustics

	Wave aberration germs	Critical set	Cusp of Gauss
Fold	$x^3 + y^2$	$x = 0$	None
Cusp	$x^4 + y^2$	$x = 0$	$x = 0$
Swallowtail	$x^5 + y^2$	$x = 0$	$x = 0$
Hyperbolic umbilic	$x^3 + xy^2$	$y = \pm\sqrt{3x}$	$x = 0$ $y = 0$
Elliptical umbilic	$x^3 - xy^2$	$x = 0$ $y = 0$	$x = 0$ $y = 0$

Table 3 provides the equations for the caustic curves for the wave aberration germs of the five elementary catastrophes and its out-of-focus perturbations, its critical set and the cusp of Gauss associated with them.

Finally, Figure 6 shows the plots of caustic curves of Table 3 for the hyperbolic and elliptical umbilical catastrophes (the rest of the cases are straight lines). Notice that the analysis in this part of the section deals with the canonical forms of the elementary catastrophes. Therefore, the variables are dimensionless. Of course, when dealing with actual wave aberrations in the rest of the paper we use proper dimensional variables and coefficients.

We argued in the previous section that the most likely wave aberration germ giving rise to PSF cores is that associated with out-of-focus hyperbolic caustics. The equations derived above prove that such a wave aberration germ produces a caustic pattern comprising a pair of hyperbolic critical curves close to a cusp of Gauss. Although the algebraic formula in Table 3 was derived for the canonical forms of the caustics, their basic features are preserved under a smooth change of variables. Recall that the caustic curves are precisely the image of the critical curves under the ray-mapping Equation (2); that is, the caustic curves are obtained propagating to the image plane those rays located at the critical set of the exit pupil. Similarly, each cusp of Gauss is mapped by Equation (2) into a point at the observation (retina) plane that we denote Y. Now, if the two branches of the hyperbolae of the hyperbolic umbilic critical curves are very close to each other, and thus also to the cusp of Gauss between them, the same must hold for the distance between the cusp and smooth curve branches of the associated caustic curves and for the associated Y, as can be deduced, for example, in Table 3 or Figure 5. While the maximal intensity takes place at the caustic curve, the fact that the cusp of Gauss and smooth curve branches are very close to each other suggests that, provided the distance is comparable to the fringe size (determined by the Berry index), the intensity near *Y* will be a product of two high intensities (determined by the Arnold index). Calculus arguments, not detailed here, show that a PSF core would emerge near point Y.

Notice that since *G* is a smooth function, there is only a finite number of discrete cusps of Gauss. An interesting property of the fertile cusps of Gauss is that they are saddle points of *G*, that is points where the gradient of *G* is zero but *G* has neither a maximum nor a minimum value. This can be verified, for example, from the explicit formula in Table 2. This property is preserved under perturbations. While in general there might be several cusps of Gauss for a curvature *G* function map of a given WFE, we need only consider those saddle points as candidates to be fertile. We shall demonstrate this feature in the examples of diplopia and triplopia.

TABLE 2 Out-of-focus wavefront error function (WFE) germs, its critical set and the cusps of Gauss for the five elementary catastrophe caustics. Positive values of δ provide imaginary values for x and therefore are not valid solutions

	Perturbed WFE germ	Critical set	Cusp of Gauss
Fold	$x^3 + y^2 + \delta(x^2 + y^2)$	$x = \frac{-\delta}{3}$	None
Cusp	$x^4 + y^2 + \delta(x^2 + y^2)$	$x = \pm\sqrt{\frac{-\delta}{6}}$	$x = 0$
Swallowtail	$x^5 + y^2 + \delta(x^2 + y^2)$	$x = \left(\frac{-\delta}{10}\right)^{1/3}$	$x = 0$
Hyperbolic umbilic	$x^3 + xy^2 + \delta(x^2 + y^2)$	$y^2 = \delta^2 + 4\delta x + 3x^2$	$x = \frac{-2\delta}{3}$ $y = 0$
Elliptical umbilic	$x^3 - xy^2 + \delta(x^2 + y^2)$	$y^2 = \delta^2 + 2\delta x - 3x^2$	$x = \frac{\delta}{3}$ $y = 0$

Therefore, the computation of an overall WFE singular point analysis (computation of critical and cusp of Gauss points) detects caustic patterns and can predict a possible generation of a PSF core. We note the important property that this WFE germ can be expressed as a linear combination of some Zernike polynomials: tilt (Z_1^1), defocus (Z_2^0) and coma (Z_3^1). Thus, any time that the local vicinity around a cusp of Gauss is dominated by a combination of those terms, we can predict the possible generation of a PSF core. The WFE associated with an out-of-focus elliptical caustic is a linear combination of defocus (Z_2^0) and trefoil coma (Z_3^3).

EXAMPLES OF DIPLOPIA AND TRIPLOPIA

In this section, we provide two examples of wave aberration functions generating polyplopia. In both cases, WFE functions are simple combinations of up to fourth-order Zernike aberration polynomials, thus implying that they might be 'natural' human eye wave aberrations that are dominated by the 2nd- to 4th-order aberrations.[37] We qualitatively evaluate the ghosting effects introduced by these examples by means of computing the wave optics PSF (through Fourier optics[1]) and retinal images simulated by convolution of those PSF with reference images. To analyse the locations of the PSF cores, we will also show the caustic patterns and the mapping of the cusps of Gauss at the retinal plane. Additionally, we provide the geometrical optics PSFs, which are the energy flux estimated by the Jacobian of the ray mapping (where infinities of the caustics are avoided by thresholding and local integration).[14,15] Zernike aberration functions conform to the ANSI standard[11] with numerical coefficients in microns.

The first example is a WFE generating diplopia and given by:

$$W = -0.5\,Z_2^0 + 0.4\,Z_2^{-2} + 0.1\,Z_4^0, \quad (5)$$

defined in a pupil radius of 3 mm.

We carried out a singular point analysis of the WFE given by Equation (5) in Figure 7. It shows the G function map and the critical set (red lines), cusp of Gauss (green dots) and umbilical points (cyan dots). There are five cusps of Gauss points (A-B-C-D-E), of which only two (A and E) are close to the critical lines.

These two fertile cusps of Gauss are the geometrical signatures of the presence of two wave aberration germs giving rise to two PSF cores. It is easy to observe from Figure 7 that these points are indeed saddle critical points of the absolute value of the G function as predicted. Figure 8 shows the caustic curves (red curves) at the retinal plane and the mapping of the cusp of Gauss (green dots), and at its side, the PSF associated with Equation (5). Geometrical optics and physical optics calculations of the PSF are juxtaposed in Figure 8 to emphasise a point noted earlier that, according to wave optics, intensity along a caustic is not uniform.[17,18] Nevertheless, both optical models show a PSF that clearly contains two intensity cores corresponding to the cusp of Gauss A and E. It is also clear (by comparison with Figure 6) that the caustic events generating them are out-of-focus hyperbolic caustics.

We note that if the pupil in this example constricts from 3-mm radius to 2 mm, then the critical points A and E in Figure 7 will lie outside the pupil and therefore make no contribution to the retinal image. The resulting PSF is the same annulus of light as Figure 8, but without the two high-intensity cores at the ends of the major axis of the ellipse. This example demonstrates that normal physiological constriction of the pupil can eliminate diplopia, for the same reason it eliminates starburst caustics[30,31] that exist when the pupil is dilated. We take advantage of this observation in the Discussion to propose a possible treatment to eliminate ghosting.

A method for detecting an out-of-focus hyperbolic umbilical WFE germ by analysing locally the G function around a cusp of Gauss is illustrated in Figure 9. On the left part, we show the global G function map of the diplopia example. Only one of the fertile cusps of Gauss (point A) is marked with a green dot. We then selected a local circular region of 0.4-mm radius around that cusp of Gauss, and plotted its G function and critical set in the right part of the Figure. A direct comparison with the elementary critical line patterns of Figure 5 shows that effectively the WFE behaves locally as an out-of-focus hyperbolic umbilical WFE in that region.

A simulated retinal image of an eye chart (Figure 10a) computed for an eye with a diplopic PSF (Figure 8) is shown

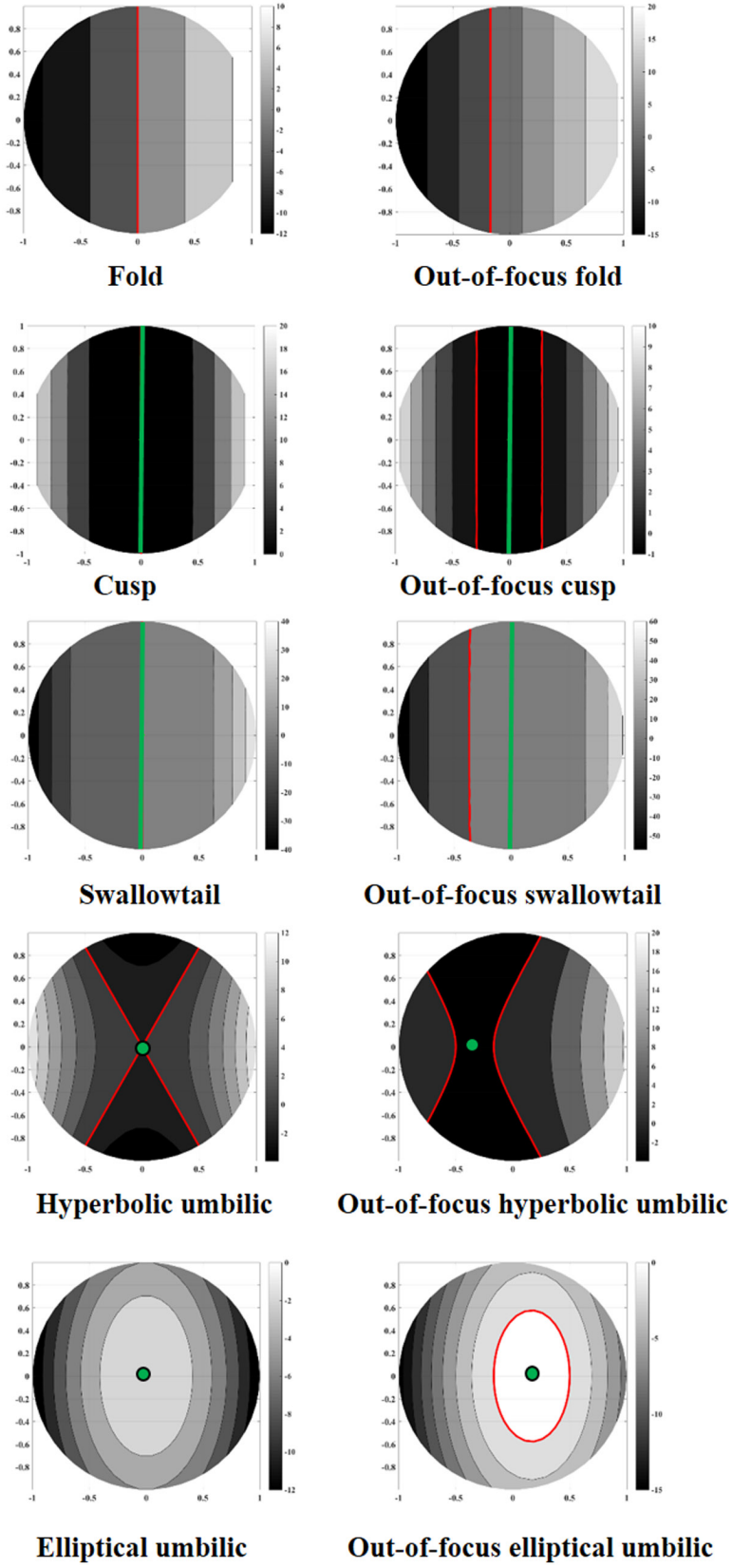

FIGURE 5 *G* function maps for each elementary catastrophe and out-of-focus perturbation of it. The critical set is plotted with red lines and the cusp of Gauss with green dots or lines.

TABLE 3 Caustic curves for the elementary wave aberration germs of the five elementary catastrophes and its out-of-focus perturbations

	In-focus WFE	Out-of-focus WFE
Fold	$\xi = 0$	$\xi = \frac{\delta^3}{3}(4-\delta)$
Cusp	$\xi = 0$	$\xi = \pm\frac{5\sqrt{6}}{9}(-\delta)^{3/2}$
Swallowtail	$\xi = 0$	$\xi = \frac{7}{2(10)^{1/3}}(-\delta)^{4/3}$
Hyperbolic umbilic	$\eta = \pm\frac{\xi}{\sqrt{3}}$	$\xi = -6x^2 - 6\delta x - \delta^2$ $\eta = \pm 2(x+\delta)^{\frac{3}{2}}\sqrt{3x+\delta}$
Elliptical umbilic	$\xi = 0$ $\eta = 0$	$\xi = -6x^2 - 2\delta x + \delta^2$ $\eta = \pm 2(x-2\delta)\sqrt{\delta^2 - 2\delta x - 6x^2}$

Note: Negative values under square roots imply imaginary solutions, which in physical terms means that the critical set is empty; that is, there are no critical points.

Abbreviation: WFE, wavefront error function.

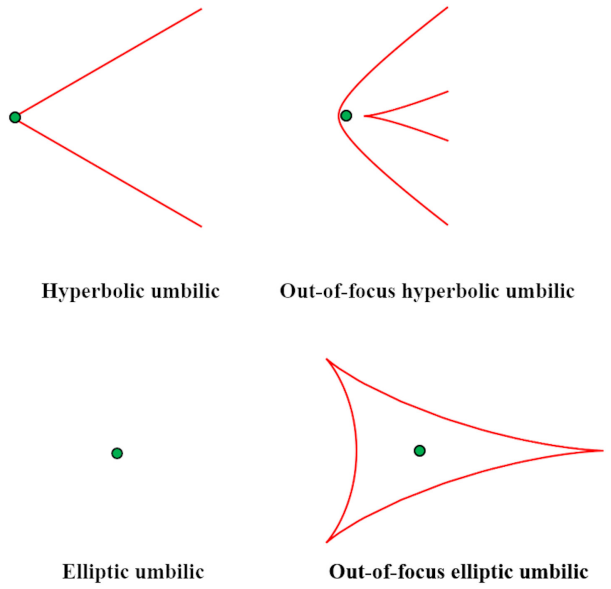

FIGURE 6 Caustic curves (red) for hyperbolic and elliptical umbilical catastrophe and perturbation of it. The mapping of the cusp of Gauss at the observation plane is plotted with green dots.

in Figure 10b. Because the PSF has two cores of equal intensity, convolution of the PSF with the letter chart produces two copies of the letter chart with the same contrast, a phenomenon clinically called 'ghosting'. Notice that the centre-to-centre separation of each letter and its ghost is equal to the separation between PSF cores, independent of letter size. Consequently, ghosting may have a minor effect on legibility for small letters that do not overlap with their ghost, but a larger effect on legibility for larger letters that partially overlap their ghosts. This is a seemingly paradoxical situation compared with normal clinical experience, in which optical blurring has a greater effect on small letters than on large letters.

The second example, shown in Figure 11, is a WFE that generates triplopia and is given by:

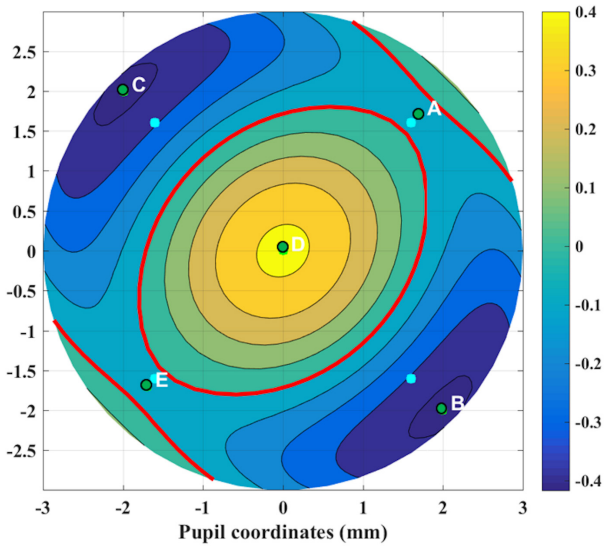

FIGURE 7 *G* function map (mm^{-2}) with singular point analysis of the diplopia example. The critical set is plotted with red lines. The cusp of Gauss and umbilical points are denoted with green and cyan dots, respectively.

$$W = 0.2\,Z_2^0 - 0.27\,Z_3^3 + 0.3\,Z_4^0, \tag{6}$$

defined in a pupil radius of 3 mm. The combination of trefoil and spherical aberration in lenses, which has been reported in some cases of mild nuclear cataracts, has been hypothesised as a cause of monocular triplopia.[7]

Figure 11 shows the *G* function map and, above it, the critical set (red lines), cusp of Gauss (green dots), and umbilical points (cyan dots).

There are seven cusps of Gauss points, of which only three (B, E and F) are close to the critical lines. Again, notice these are the only cusps of Gauss that are critical saddle points of the *G* function. Figure 12 shows the caustic curves (red curves) at the retinal plane and the mapping of the cusps of Gauss (green dots) and at its side the PSF associated with Equation (6). Now, the PSF presents six intensity cores. However, three of them are brighter than the other three, specifically, those associated with cusps of Gauss marked by letters B, E and F. As in the diplopia example, it is also clear (by comparison with Figure 6) that the caustic events generating them are out-of-focus hyperbolic caustics. The other three, less intense, peaks are due to the crossing of fold caustics. However, as we already discussed when describing the swallowtail caustic, these intersections do not involve new catastrophes because the coalescing rays come from distinct parts of the wavefront.[20] This explains why the intensity at those points is slightly lower.

Convolution of the PSF in Figure 12 with the letter chart in Figure 13a results in a strongly degraded image shown in Figure 13b for which letters of all sizes are difficult to identify. This optical effect is important functionally because poor letter recognition due to changes in spatial form of

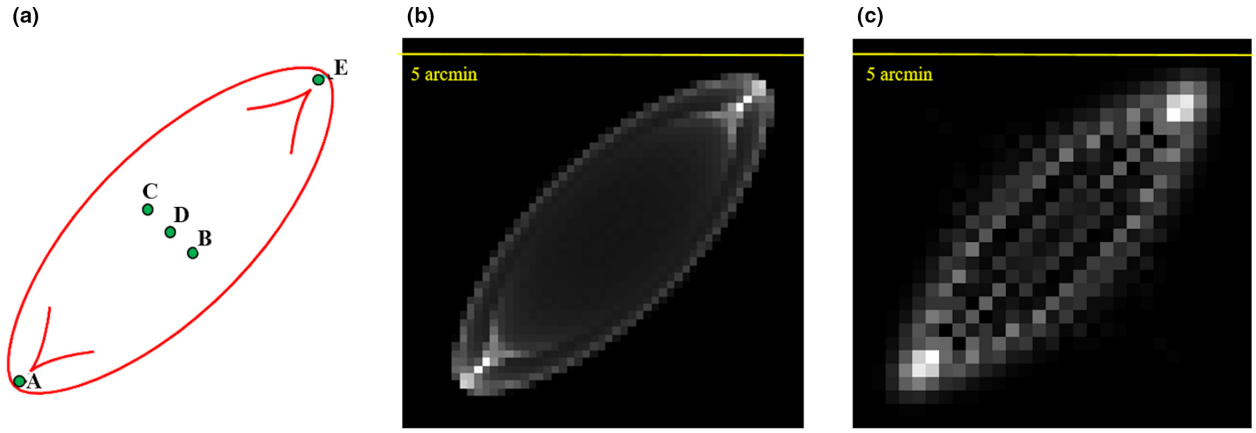

FIGURE 8 (a) Caustic pattern plot of the diplopia example. Mapping of the cusps of Gauss at the retinal plane is denoted with A-E green circles. Only two of them are fertile cusps of Gauss: A and E. In addition, (b) the geometrical optics point spread function (PSF) and (c) the wave optics PSF. Dimensions of PSF are given in arcmin.

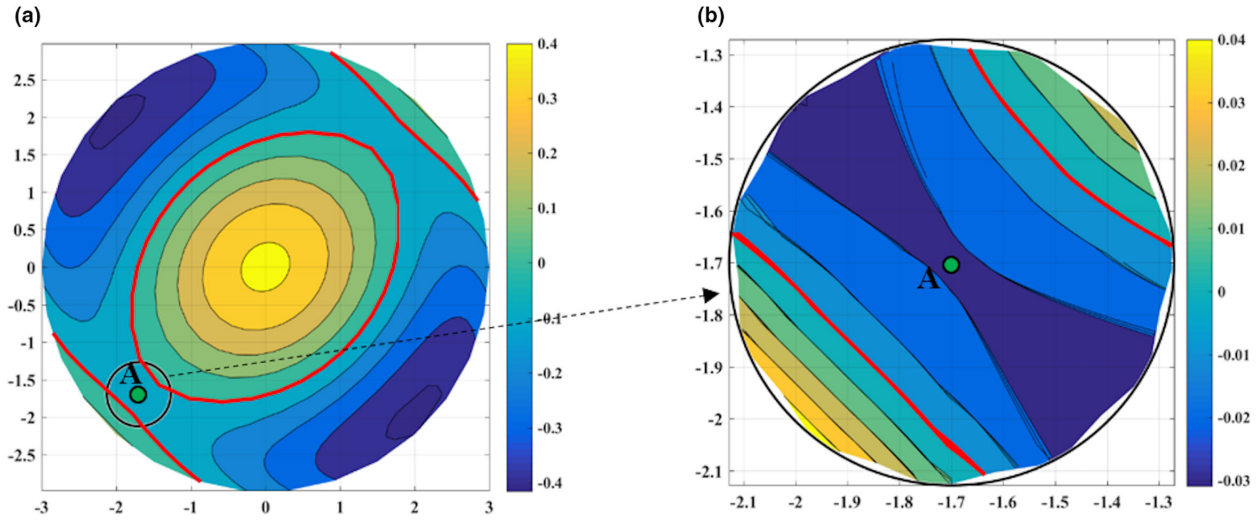

FIGURE 9 (a) *G* function map (mm^{-2}) with the critical set (red lines) and the fertile cusp of Gauss A for the whole pupil (3 mm) of the diplopia example. (b) *G* function map (mm^{-2}) of a 0.4-mm circular region centred at the fertile cusp of Gauss A of the diplopia example.

text, in turn, impacts word recognition, which has consequences for further linguistic processing by the visual system and the strategic programming of eye movements during active reading.[38]

ON THE THEORETICAL POSSIBILITIES OF POLYPLOPIA CORRECTION THROUGH PHASE-MASKING TECHNIQUES

The results presented above suggest that eliminating the WFE regions giving rise to PSF cores could be applied to correct polyplopia. Here, we explore, through computer simulations, the potentials of a phase-masking technique for this purpose.

We simulated the effect of introducing an amplitude circular binary mask (amplitude takes one value inside and zero outside) centred on one fertile cusp of Gauss that multiplies the pupil function. We applied it for the diplopia example presented in the previous section. Figure 14 shows the resulting PSF and its convolution with a reference image for different values of the mask circular radius.

Figure 14 clearly shows that diplopia perception is cancelled using a mask around one of the fertile cusps of Gauss (point E). However, such a mask also introduces undesired effects. Besides the decrease in image contrast due to energy loss, a small circular mask also induces a typical Airy disk diffraction pattern (Figure 14a), then blurring the image too much. This leads to a trade-off problem about the size of the mask as a design parameter. In this specific example, the optimum mask size is a value around 2.5 mm, as revealed by Figure 14.

However, one may argue the following: Would it not be possible to obtain the same results by centring the mask at the pupil centre? If such a mask were small enough to block

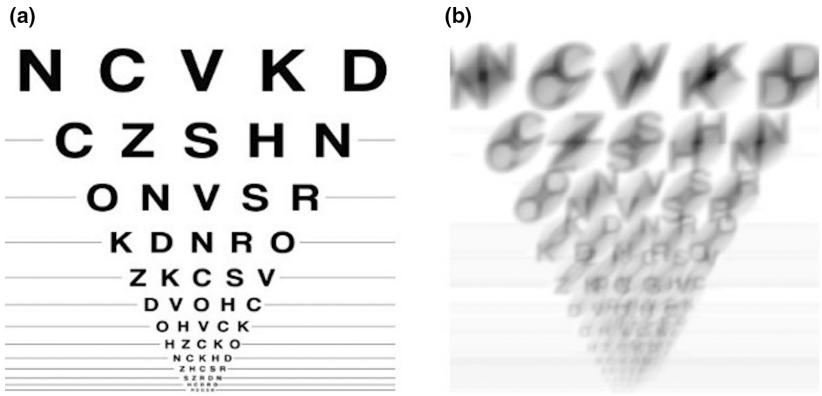

FIGURE 10 (a) Reference image; (b) convolved reference image with the point spread function (PSF) of wavefront error function (WFE) given by Equation (5), that is the diplopia example.

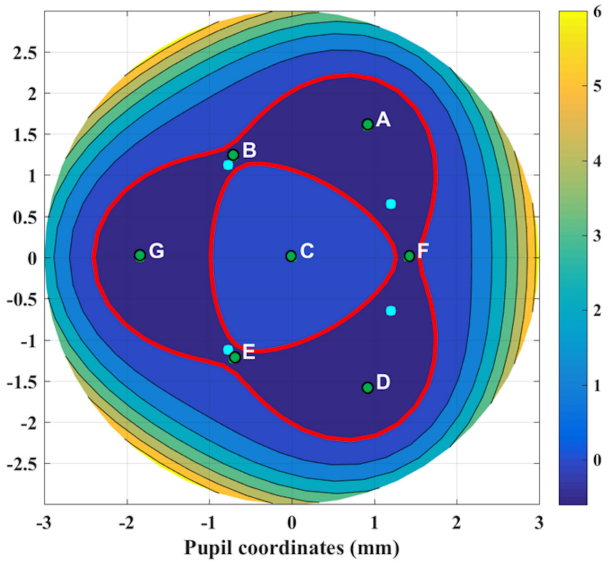

FIGURE 11 *G* function map (mm^{-2}) with singular point analysis of the triplopia example. The critical set is plotted with red lines. The cusp of Gauss and umbilical points are denoted with green and cyan dots, respectively.

the two fertile cusps of Gauss, it would also prevent diplopia at the expense of losing considerable light flux. To reveal the advantages of centring the circular mask around a fertile cusp of Gauss instead of at the pupil centre, we computed the PSFs and convolved images with the optimum mask of 2.5 mm centred now at the pupil centre. Figure 15 shows the results. Although the centring at the pupil centre effectively cancels diplopia by stopping most of the energy that forms the main image, the image with the mask at the centre of the pupil shows slightly worse contrast as compared to the mask centred at the fertile cusp of Gauss. The reason is that centring at the cusp of Gauss optimises the amount of energy not blocked by the mask and therefore implicitly optimises image contrast with respect to centring the same mask in any other location of the pupil.

EXPERIMENTAL GENERATION OF DIPLOPIA AND TRIPLOPIA EXAMPLES

An optical system has been used to test the theoretical predictions of multiplopia generation. Figure 16 shows a schematic sketch of the set-up used here, which

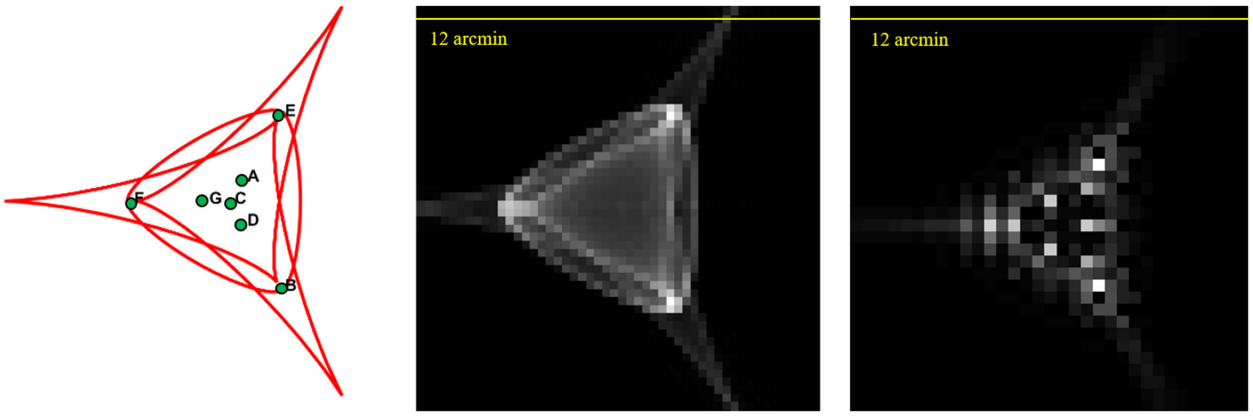

FIGURE 12 (a) Caustic pattern plot of the triplopia example. Mapping of the cusps of Gauss at the retinal plane is denoted with A-G green circles. Only three of them are fertile cusps of Gauss: B, F and E. In addition: (b) the geometrical optics point spread function (PSF) and (c) the wave optics PSF. Dimensions of PSF are given in arcmin.

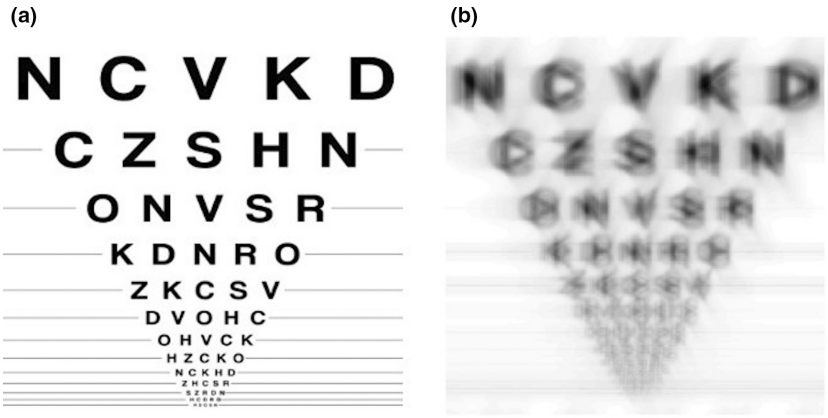

FIGURE 13 (a) Reference image; (b) convolved reference image with the point spread function (PSF) of wavefront error function (WFE) given by Equation (6), that is the triplopia example.

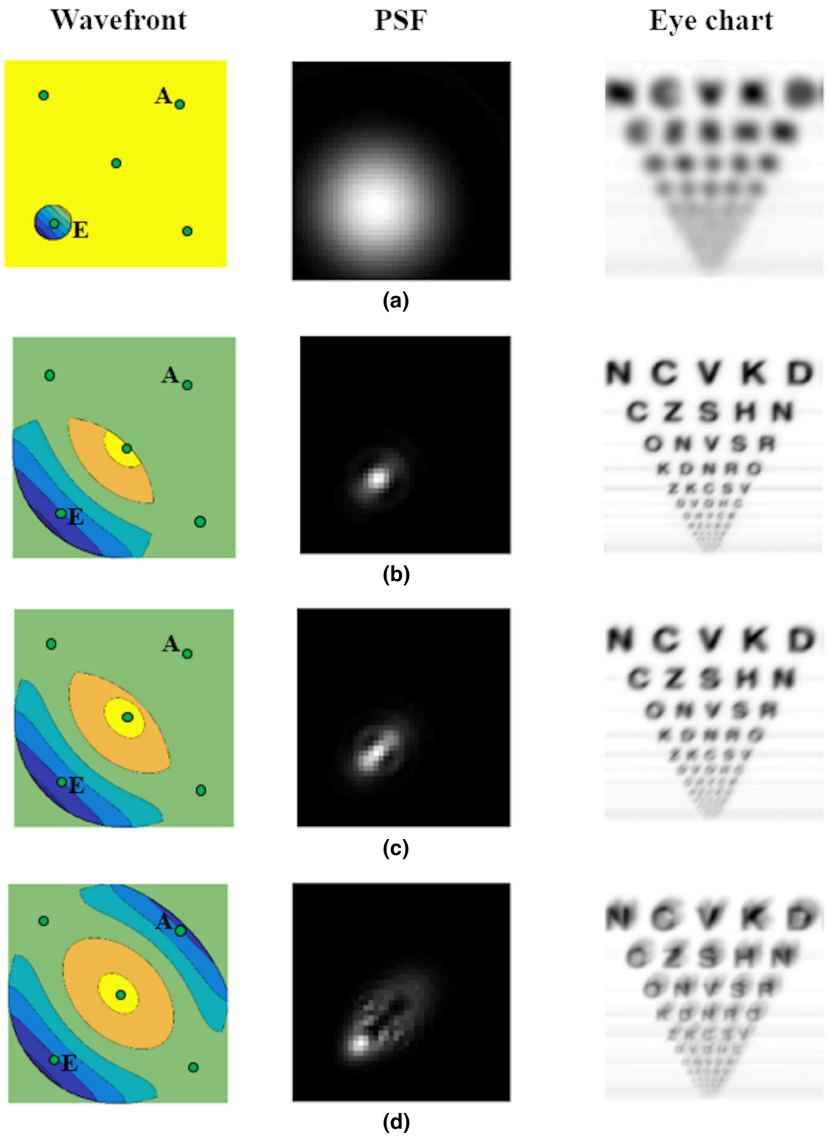

FIGURE 14 Wavefronts with the circular masking around the cusp of Gauss E (the two fertile cusps of Gauss are green dots E and A), point spread functions (PSFs) and convolved images (eye chart) in the diplopia example using circular masks of radius size: (a) 0.5 mm, (b) 2.5 mm, (c) 3 mm and (d) 5 mm. Diplopia starts to appear in case (d) because the second fertile cusp of Gauss (point A) in that case is not blocked.

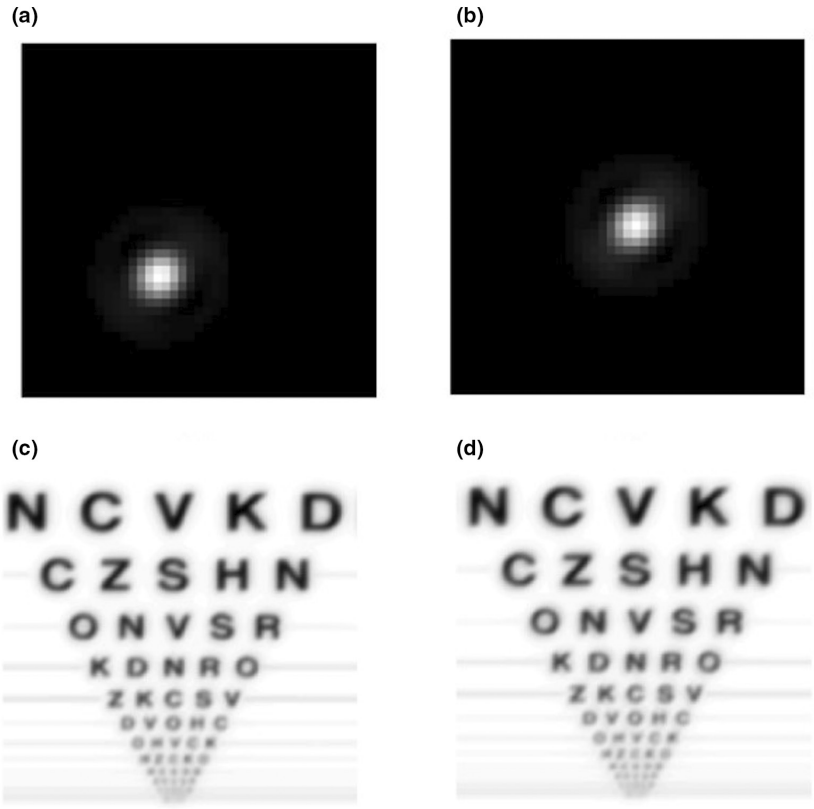

FIGURE 15 Point spread function (PSF) (a, b) and convolved images (c, d) in the diplopia example using a circular mask of size 2.5 mm centred at a fertile cusp of Gauss (a–c) or the pupil centre (b–d).

is similar to the system described previously.[39,40] A CCD camera (DC1645C-HQ, Thorlabs, thorlabs.com) with an objective (AF NIKKOR 85 mm, Nikon, Nikon.com) was used instead of an eye, to record the image of the eye chart generated in a microdisplay, and a beam splitter and a similar camera placed near the wavefront sensor to capture the PSF created by a laser with a wavelength of 633 nm.

To generate the wavefronts of Equations (5) and (6), firstly the deformable mirror corrected the small aberrations of the system itself with a remaining total RMS of 0.039 microns for a 8.75-mm pupil. Secondly, the pupil was reduced to 6 mm (remaining total RMS of 7 nm) and the aberrations corresponding to Equation (5) (diplopia) and Equation (6) (triplopia) were generated. The error in the generation of the Zernike coefficients of Equations (5) and (6) is within the order of nanometres, obtaining a residual RMS wavefront error (RMS of the difference between the nominal and the generated wavefront) for the diplopia and triplopia generation of 0.07 and 0.11 microns, respectively.

Figure 17 shows the PSFs of the WFEs given by Equation (5) and Equation (6) and the associated eye-chart images generated in a microdisplay.

PSF images obtained experimentally (Figure 17) show large concentrations of light at the small areas of the image predicted by the theory and computer simulations (see Figures 8 and 12). Eye-chart images show the generated diplopia and triplopia, which is especially visible in those letters small enough to separate the ghost images. In the case of diplopia, the lower ghost letter has a higher contrast because the corresponding PSF is slightly more intense.

DISCUSSION

Monocular polyplopia and its optical origins were already described in the late nineteenth century. As early as 1896, Bull[2] stated that the perception of multiple images must be traced to the distribution of the salient elements of light and darkness in the 'star', which is characteristic of the observed eye. When Bull writes 'star', he is referring to the caustic pattern perceived by the human eye when a star is seen; what now is called 'starburst'.[18,30,31] Bull and Verhoff[12] were already tracing the origin of multiple images to some caustic intensity features. Their intuition predates the mathematical theory developed of this paper that reveals how optical aberrations contribute to the perception of multiple images.

Early efforts by Verhoeff[12] to connect caustics to perceived diplopia employed the familiar example of a radially symmetric system with positive spherical aberration and negative (hyperopic) defocus that produces an annular ring caustic in the retinal plane. To generate diplopia, Verhoff introduced a meridional aperture that isolated two cores along the annular PSF (see Figure 1 in Verhoff). The

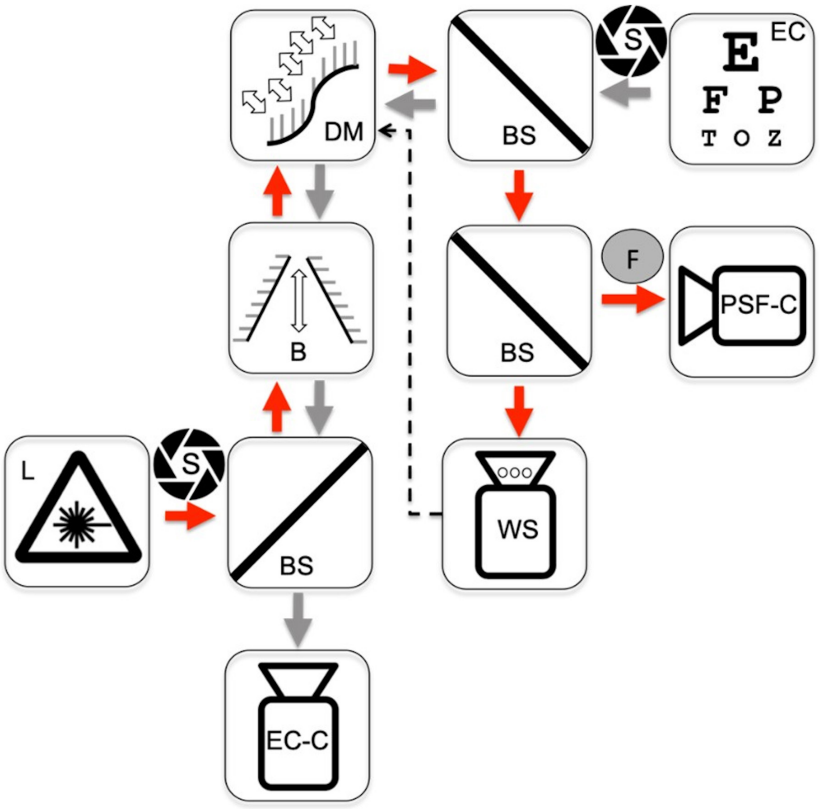

FIGURE 16 Schematic of the experimental set-up. L, laser; BS, beam splitter; B, Badal system; DM, deformable mirror; WS, wavefront sensor; EC, eye chart; PSF-C, PSF image camera; EC-C, eye-chart image camera; S, stop; and F, neutral density filter. The dotted line indicates the closed-loop operation mode. Red arrows show the path of the laser light, while grey arrows show the path of the light emitted by the microdisplay.

annular caustic produced by spherical aberration is created by ray crossings at the perimeter of the beam of light passed by the pupil (Figure 2 in Verhoff), and may be seen in almost every entoptic PSF reported by Tscherning[41] (e.g., figures 85–92). This common entoptic observation is understandable given the ubiquity of positive spherical aberration in human eyes[37] and the commonplace hyperopic defocus created by either hyperopia, presbyopia and/or accommodative lag. In the absence of other higher-order aberrations, the combination of positive spherical aberration and negative defocus will not generate isolated fertile cusps of Gauss, and therefore will not create the multiple, discrete PSF cores examined in this report. Nevertheless, the retinal image will be corrupted in a way that superficially resembles diplopia. Convolution of an elliptical ring PSF with objects containing straight lines and edges (e.g., a clinical letter chart) will smear the retinal image continuously due to the superposition of a multitude of copies of the object. Fortunately, image degradation created in this way can be prevented by a conventional ophthalmic lens that either corrects the hyperopia, or provides the presbyopic eye with sufficient additional power to focus near targets.

One motivation for the present study was to explore the possibility that optical analysis of caustics in the PSF will reveal ways to predict the presence and number of multiple retinal images to be expected for an eye with known wavefront aberrations. Using the mathematical concepts and tools of catastrophe theory, we have shown that computation of fertile cusps of Gauss from the eye's wavefront aberrations can predict the generation of PSF cores responsible for polyplopia. The number and location of these cores are thus a potentially useful metric for the existence and severity of polyplopia in spatial vision. Moreover, we have shown that the most likely event giving rise to PSF cores is associated with out-of-focus hyperbolic, or less probably elliptical, caustics. It is worth mentioning that recently it has been proved that the hyperbolic umbilic caustic is a stable catastrophe caustic in its free propagation along the propagation axis.[27]

We have shown that the wave aberration germ generating the hyperbolic caustic comprises a pair of hyperbolic critical curves close to a cusp of Gauss. Therefore, such local patterns within the global wave aberration can be used to identify and describe the appearance of PSF cores. The proximity of pairs of hyperbolic critical curves will determine their impact on vision quality, something to be quantified through computational simulations or visual optics experiments.

We point out the peculiar fact, proven in the singular analysis of elementary catastrophe germs, that while a geometrical optical analysis reveals the presence of multiple PSF cores, the precise location and intensity of local maxima of a PSF are determined by the diffractive pattern of the caustic. We might say that geometrical optics,

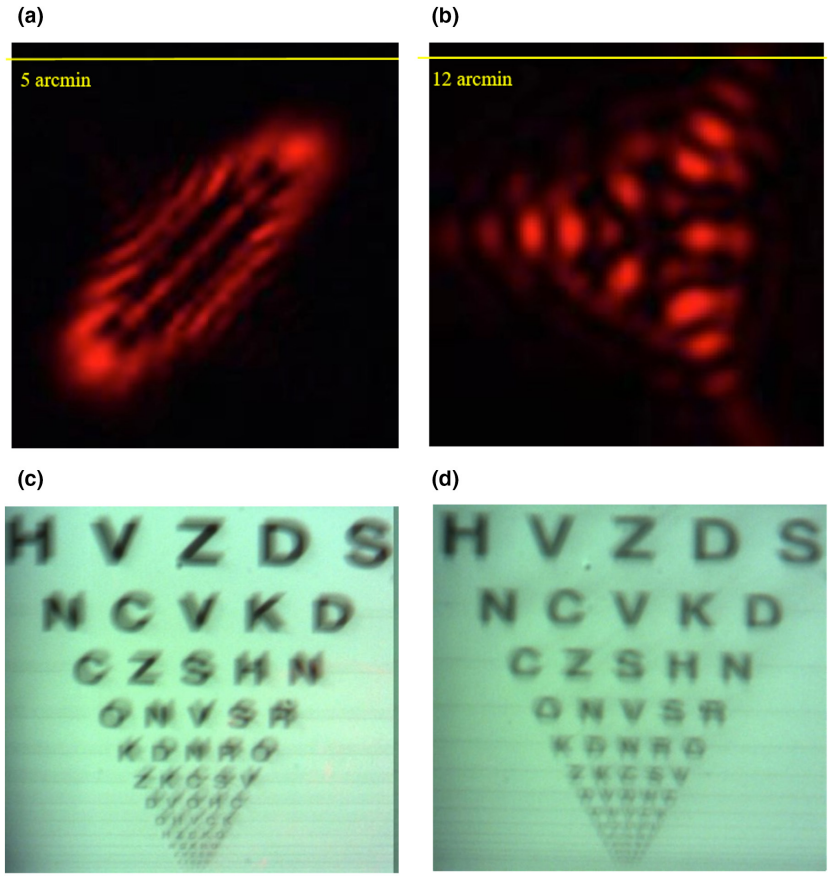

FIGURE 17 Experimentally recorded point spread functions (PSFs) of the wavefront error functions (WFEs) given by Equations (5) and (6), generating diplopia (a) and triplopia (b), respectively. Eye-chart images for the diplopia (c) and the triplopia (d) examples.

as explained by the stationary phase principle, provides the 'bone structure' of the PSF and wave optics the 'flesh'. These details of the PSF structure[42] are not just secondary effects but are essential determinants of PSF maxima. For this reason, our investigation of polyplopia relied mainly upon physical, not geometrical, optical analysis.

Comparing our computer simulations and experimental recordings, we observe that the match between theory and the experiment is high although not perfect (especially for triplopia), perhaps because the experiment used a deformable mirror with just 52 actuators, generating a WFE that contains some residual aberrations with respect to the one that was being simulated. Small deformations of the wavefront can induce changes in the intensity of the PSF cores, thereby affecting contrast of the multiple images.

Our discovery of the local geometrical features generating ghosting opens new potential strategies to relieve the visual asthenopia associated with ghosting. The appearance of multiple different images (often one in-focus and the other out of focus) is a familiar experience of presbyopic or pseudophakic patients fitted with multifocal corrections.[43–45] It has been proposed[46] that the visual impact of ghost images can be reduced by controlling levels of spherical aberration within multifocal lens designs. As revealed in Figures 1, 8, 10, 12, 13 and 17, and associated with Equations (5) and (6), polyplopia is most striking when opposite sign defocus and spherical aberration are combined with, for example, astigmatism (Equation (5)) or trefoil (Equation (6)), and therefore, polyplopia may be avoided by ensuring that spherical aberration and defocus share the same sign.[47]

Our analysis reveals two possible strategies for avoiding multiple images based on either wavefront phase manipulation,[48,49] or some customisation of the pupil amplitude function, for example masking those regions of the pupil[50–52] responsible for the extra PSF cores. To be successful, the masking strategy must resolve collateral effects of reduced retinal illuminance and added diffraction associated with mask edges. Diffraction effects of small masks can be ameliorated by applying Gaussian rather than binary transmission transitions. The pupil-masking technique could be implemented using artificial apertures included within contact lenses,[53] the cornea (e.g. corneal inlays[54] or tattoos[55]) or intraocular lenses containing opaque outer regions.[52,56]

ACKNOWLEDGEMENTS

This work was supported by grant PID2020-113596GB-I00 from the Spanish Ministerio de Ciencia e Innovacion and from the Israel Science Foundation. We are also very thankful to the two anonymous reviewers who, with their sharp comments, have contributed significantly to a better presentation of this report.

AUTHOR CONTRIBUTIONS

Sergio Barbero: Conceptualization (lead); software (lead); writing – original draft (lead). **Arthur Bradley:** Conceptualization (equal); methodology (equal); supervision (equal); writing – review and editing (equal). **N Lopez-Gil:** Conceptualization (equal); data curation (equal); methodology (equal); resources (equal); software (equal); supervision (equal); writing – review and editing (equal). **Jacob Rubinstein:** Conceptualization (equal); investigation (equal); methodology (equal); supervision (equal); writing – review and editing (equal). **Larry Thibos:** Conceptualization (equal); investigation (equal); methodology (equal); software (equal); supervision (equal); visualization (equal); writing – review and editing (equal).

CONFLICTS OF INTEREST

The authors report no conflicts of interest.

ORCID

Sergio Barbero https://orcid.org/0000-0003-4555-4114
Norberto López-Gil https://orcid.org/0000-0002-6696-4596
Jacob Rubinstein https://orcid.org/0000-0002-3295-1957
Larry Thibos https://orcid.org/0000-0002-3726-3344

REFERENCES

1. Goodman JW. Introduction to Fourier optics. 3rd ed. Greenwood Village, CO: Roberts & Co; 2005. p. 491.
2. Bull GJ. The visual effects of refractive errors. *Trans Ophthalmol Soc U K*. 1896;16:200–47.
3. Carney LG, Liubinas J, Bowman KJ. The role of corneal distortion in the occurrence of monocular diplopia. *Acta Ophthalmol*. 1981;59:271–4.
4. Bowman KJ, Smith G, Carney LG. Corneal topography and monocular diplopia following near work. *Am J Optom Physiol Opt*. 1978;55:818–23.
5. Goss DA, West RW, Carr LW, Edmondson LL. A case of monocular triplopia of lenticular origin. *Optom Vis Sci*. 1992;69:486–8.
6. Campbell C. Observations on the optical effects of a cataract. *J Cataract Refract Surg*. 1999;25:995–1003.
7. Kim A, Bessho K, Okawa Y, Maeda N, Tano Y, Hirohara Y, et al. Wavefront analysis of eyes with cataracts in patients with monocular triplopia. *Ophthalmic Physiol Opt*. 2006;26:65–70.
8. Bour L, Apkarian P. Segmented refraction of the crystalline lens as a prerequisite for the occurrence of monocular polyplopia, increased depth of focus, and contrast sensitivity function notches. *J Opt Soc Am A*. 1994;11:2769–76.
9. Bradley A, Xu R, Thibos L. Optical basis of polyplopia. *J Vis*. 2013;13:T1. https://doi.org/10.1167/13.15.1
10. Gaskill JD. Linear systems, Fourier transforms, and optics. New York, NY: John Wiley & Sons; 1978. p. 71–4.
11. ANSI. American National Standards Institute. American National Standard Z80.28 for ophthalmics – methods for reporting optical aberrations of eyes. 2010.
12. Verhoeff FH. The cause of a special form of monocular diplopia. *Arch Ophthalmol*. 1900;29:565–72.
13. Campbell C. Corneal aberrations, monocular diplopia, and ghost images: analysis using corneal topographical data. *Optom Vis Sci*. 1998;75:197–207.
14. Mahajan VN. Optical imaging and aberrations. Bellingham, WA: SPIE Optical Engineering Press; 1998.
15. Thibos LN. Calculation of the geometrical point-spread function from wavefront aberrations. *Ophthalmic Physiol Opt*. 2019;39:232–44.
16. Born M, Wolf E. Principles of optics. 4th ed. Oxford: Pergamon Press; 1970.
17. Berry MV, Upstill C. IV catastrophe optics: morphologies of caustics and their diffraction patterns. Progress in optics. Volume 18. Amsterdam: Elsevier; 1980. p. 257–346.
18. Rubinstein J. On the geometry of visual starbursts. *J Opt Soc Am A*. 2019;36:B58–64.
19. Poston T, Stewart I. Catastrophe theory and its applications. London: Pitman; 1978.
20. Nye JF. Natural focusing and fine structure of light. Bristol: Institute of Physics Publishing; 1999. p. 328.
21. Charman WN, Heron G. Microfluctuations in accommodation: an update on their characteristics and possible role. *Ophthalmic Physiol Opt*. 2015;35:476–99.
22. Porteous IR. Geometric differentiation: for the intelligence of curves and surfaces. Cambridge: Cambridge University Press; 2001.
23. Banchoff T, Gaffney T, McCrory C. Cusps of Gauss mappings. London: Pitman; 1982.
24. Thom R. Stabilité structurelle et morphogénèse. Paris: Interédition; 1974.
25. Arnold VI. Catastrophe theory (translated by RK Thomas). Berlin: Springer-Verlag; 1984. p. 79.
26. Zannotti A, Denz C, Alonso MA, Dennis MR. Shaping caustics into propagation-invariant light. *Nat Commun*. 2020;11:1–7.
27. Espíndola-Ramos E, Silva-Ortigoza G, Sosa-Sánchez CT, Julián-Macías I, de Jesús C-RO, Ortega-Vidals P, et al. Paraxial optical fields whose intensity pattern skeletons are stable caustics. *J Opt Soc Am A*. 2019;36:1820–8.
28. Berry MV. Waves and Thom's theorem. *Adv Phys*. 1976;25:1–26.
29. Whitney H. On singularities of mappings of Euclidean spaces. I. Mappings of the plane into the plane. *Ann Math*. 1955;62:374–410.
30. Xu R, Kollbaum P, Thibos L, Lopez-Gil N, Bradley A. Reducing starbursts in highly aberrated eyes with pupil miosis. *Ophthalmic Physiol Opt*. 2018;38:26–36.
31. Xu R, Thibos LN, Lopez-Gil N, Kollbaum P, Bradley A. Psychophysical study of the optical origin of starbursts. *J Opt Soc Am A*. 2019;36:B97–B102.
32. Nye J. Symmetrical optical caustics. *J Opt*. 2018;20:075612. https://doi.org/10.1088/2040-8986/aac93c
33. Lovric M. Vector calculus. New York, NY: John Wiley & Sons; 2007.
34. Mahajan VN. In: O'Shea DC, editor. Aberration theory made simple. Bellingham, WA: SPIE Optical Engineering Press; 1991.
35. Marin-Franch I, Xu R, Bradley A, Thibos LN, Lopez-Gil N. The effect of spherical aberration on visual performance and refractive state for stimuli and tasks typical of night viewing. *J Opt*. 2018;11:144–52.
36. Barbero S, Gonzalez MDM. Admissible surfaces in progressive addition lenses. *Opt Lett*. 2020;45:5656–9.
37. Thibos LN, Hong X, Bradley A, Cheng X. Statistical variation of aberration structure and image quality in a normal population of healthy eyes. *J Opt Soc Am A*. 2002;19:2329–48.
38. Young LK, Liversedge SP, Love GD, Myers RM, Smithson HE. Not all aberrations are equal: reading impairment depends on aberration type and magnitude. *J Vis*. 2011;11:20. https://doi.org/10.1167/11.13.20
39. Bernal-Molina P, Marín-Franch I, Del Águila-Carrasco AJ, Esteve-Taboada JJ, López-Gil N, Kruger PB, et al. Human eyes do not need monochromatic aberrations for dynamic accommodation. *Ophthalmic Physiol Opt*. 2017;37:602–9.
40. Del Águila-Carrasco AJ, Marín-Franch I, Bernal-Molina P, Esteve-Taboada JJ, Kruger PB, Montés-Micó R, et al. Accommodation responds to optical vergence and not defocus blur alone. *Invest Ophthalmol Vis Sci*. 2017;58:1758–63.
41. Tscherning M. Physiologic optics. Philadelphia, PA: The Keystone Press; 1904.
42. Kravtsov YA, Orlov YI. Caustics, catastrophes and wave fields. Berlin: Springer Verlag; 1999.
43. Kollbaum PS, Dietmeier BM, Jansen ME, Rickert ME. Quantification of ghosting produced with presbyopic contact lens correction. *Eye Contact Lens*. 2012;38:252–9.

44. Fedtke C, Bakaraju RC, Ehrmann K, Chung J, Thomas V, Holden BA. Visual performance of single vision and multifocal contact lenses in non-presbyopic myopic eyes. *Cont Lens Anterior Eye*. 2016;39:38–46.
45. Venter JA, Pelouskova M, Collins BM, Schallhorn SC, Hannan SJ. Visual outcomes and patient satisfaction in 9366 eyes using a refractive segmented multifocal intraocular lens. *J Cataract Refract Surg*. 2013;39:1477–84.
46. Bradley A, Kollbaum P, Thibos LN, inventors. Multifocal correction providing improved quality of vision. USA patent US8894203, US9770326. 2014.
47. Papadatou E, Del Águila-Carrasco AJ, Marín-Franch I, López-Gil N. Temporal multiplexing with adaptive optics for simultaneous vision. *Biomed Opt Express*. 2016;7:4102–13.
48. Ares J, Flores R, Bara S, Jaroszewicz Z. Presbyopia compensation with a quartic axicon. *Optom Vis Sci*. 2005;82:1071–8.
49. Dai G-M. Optical surface optimization for the correction of presbyopia. *Appl Opt*. 2006;45:4184–95.
50. Osborn J, Myers RM, Love GD. PSF halo reduction in adaptive optics using dynamic pupil masking. *Opt Express*. 2009;17:17279–92.
51. Navarro R, Fernández-Sánchez V, López-Gil N. Refractive status in eyes with inhomogeneous or irregular pupils. *Optom Vis Sci*. 2014;91:221–30.
52. Bonaque-González S, Ríos-Rodríguez S, López-Gil N. Improving vision by pupil masking. *Biomed Opt Express*. 2016;7:2538–50.
53. Vásquez-Quintero A, Pérez-Merino P, Fernández-García AI, De Smet H. Smart contact lens: a promising therapeutic tool in aniridia. *Arch Soc Esp Oftalmol*. 2021;96:68–73.
54. Langenbucher A, Goebels S, Szentmary N, Seitz B, Eppig T. Vignetting and field of view with the KAMRA corneal inlay. *Biomed Res Int*. 2013;2013:154593. https://doi.org/10.1155/2013/154593
55. Burris TE, Holmes-Higgin DK, Silvestrini TA. Lamellar intrastromal corneal tattoo for treating iris defects (artificial iris). *Cornea*. 1998;17:169–73.
56. Thompson CG, Fawzy K, Bryce IG, Noble BA. Implantation of a black diaphragm intraocular lens for traumatic aniridia. *J Cataract Refract Surg*. 1999;25:808–13.

How to cite this article: Barbero S, Bradley A, López-Gil N, Rubinstein J, Thibos L. Catastrophe optics theory unveils the localised wave aberration features that generate ghost images. *Ophthalmic Physiol Opt*. 2022;42:1074–1091. https://doi.org/10.1111/opo.13008